Planar Cable-Direct-Driven Robots, Part II: Dynamics and Control

Paolo Gallina and **Aldo Rossi**
University of Padova
Padova, Italy

Robert L. Williams II
Ohio University
Athens, Ohio

DETC2001/DAC-21146
Proceedings of the
2001 ASME Design Technical Conferences
27th Design Automation Conference
September 9-12, 2001, Pittsburgh, PA

Contact information:

Robert L. Williams II
Associate Professor
Department of Mechanical Engineering
257 Stocker Center
Ohio University
Athens, OH 45701-2979
Phone: (740) 593-1096
Fax: (740) 593-0476
E-mail: williar4@ohio.edu
URL: http://www.ent.ohiou.edu/~bobw

Proceedings of DETC2001
2001 ASME Design Engineering Technical Conferences
September 9-12, 2001, Pittsburgh, PA

DETC2001/DAC-21146

PLANAR CABLE-DIRECT-DRIVEN ROBOTS, PART II: DYNAMICS AND CONTROL

Paolo Gallina and **Aldo Rossi**
University of Padova
Padova, ITALY

Robert L. Williams II
Ohio University
Athens, OH

ABSTRACT

A hybrid parallel/serial manipulator architecture was introduced in a companion paper where the translational freedoms are provided by a cable-direct-driven robot (CDDR) and the rotational freedoms are provided by a serial wrist mechanism. While the companion paper presents kinematics and statics, the current paper presents a dynamics model and simulated control for planar CDDRs. Examples are presented to compare the planar 3-cable CDDR with one degree of actuation redundancy and the 4-cable CDDR with two degrees of actuation redundancy. It was found that the 4-cable tracking error was worse than for the 3-cable case, due to increased inertia with an additional actuator. Also, the controller architecture considers including and not including a feedforward reference acceleration term with the overall mass matrix; the performance of the controller with the feedforward term is clearly preferable.

1. INTRODUCTION

Cable-direct-driven robots (CDDRs) are a type of parallel manipulator wherein the end-effector link is supported in-parallel by *n* cables with *n* tensioning motors. Several CDDRs and cable-direct-driven haptic interfaces (CDDHIs) have been presented by other authors and are reviewed in the companion paper (Williams and Gallina, 2001). Roberts et al. (1998), present the inverse kinematics, cable-tension-optimization, and fault tolerance of Charlotte-type (Campbell et al., 1995) CDDRs, but no dynamics modeling is presented. Sklar and Tesar (1988) present the dynamics of hybrid serial manipulators consisting of parallel joints. This manipulator architecture is significantly different from the currently-proposed hybrid parallel/serial manipulator architecture where the translational freedoms are provided by a CDDR and the rotational freedoms by a serial wrist mechanism.

CDDRs are designed with actuation redundancy, i.e. with more actuated cables than wrench-exerting degrees-of-freedom in attempt to avoid configurations where certain wrenches require an impossible compression force in one or more cables. Despite actuation redundancy, there exist subspaces in the potential workspace where some cables can lose tension. This problem can be exacerbated by CDDR dynamics, hence the current paper studies dynamics and control of planar CDDRs.

This paper reviews the two candidate planar CDDRs from the companion paper, presents dynamics modeling resulting in a nonlinear, coupled dynamics model, followed by Cartesian trajectory control simulation employing Cartesian PD control for planar CDDRs with one and two degrees actuation redundancy. This paper focuses on translational motion and forces.

2. CABLE-DIRECT-DRIVEN ROBOTS (CDDRs)

A CDDR consists of a single end-effector point supported in parallel by *n* cables controlled by *n* tensioning actuators. Figures 1 and 2 show the planar 3-cable and 4-cable CDDR diagrams. These figures are similar to the kinematics diagrams in the companion paper (Williams and Gallina, 2001), but we have added the end-effector point mass *m* and the lumped motor shaft/cable pulley rotational inertias for each actuator J_i ($i = 1, \cdots, n$). The cable pulley radius for each actuator is r_i ($i = 1, \cdots, n$; shown in Fig. 3). We also include viscous damping coefficients c_i ($i = 1, \cdots, n$) at each motor shaft to provide a linear model for the system friction.

For 2-dof planar translations there must be at least two cables. Since cables can only exert tension on the end-effector, there must be more cables to avoid configurations where the robot can be slack and lose control. Figure 1 represents one degree of actuation redundancy, i.e. three cables to achieve the two Cartesian degrees-of-freedom $\mathbf{X} = \{x \quad y\}^T$; the four-cable CDDR in Fig. 2 has two degrees of actuation redundancy. Figures 1 and 2 show the inertially-fixed reference frame $\{\mathbf{0}\}$ whose origin is the centroid of the base polygon; the regular base polygon (triangle and square, respectively) has sides of fixed length L_B; each cable is attached to the ground link at $\mathbf{A}_i = \{A_{ix} \quad A_{iy}\}^T$; the length of each cable is denoted as L_i, and the cable angles are θ_i ($i = 1, \cdots, n$).

3. CDDR DYNAMICS MODELING

This section presents dynamics modeling for planar CDDRs. Dynamics modeling is required for improved control (compared to using kinematics and statics modeling only) when CDDRs are to provide high velocities and accelerations in translational motion. Dynamics modeling is concerned with relating the Cartesian translational motion of the moving CDDR point to the required active joint torques. Due to the cable actuation, CDDR dynamics modeling is not very similar to in-parallel-actuated robot dynamics modeling (e.g. Tsai, 1999; Gosselin, 1996). Another complicating factor is that with CDDRs the joint space is overconstrained with respect to the Cartesian space due to the redundant actuation.

.

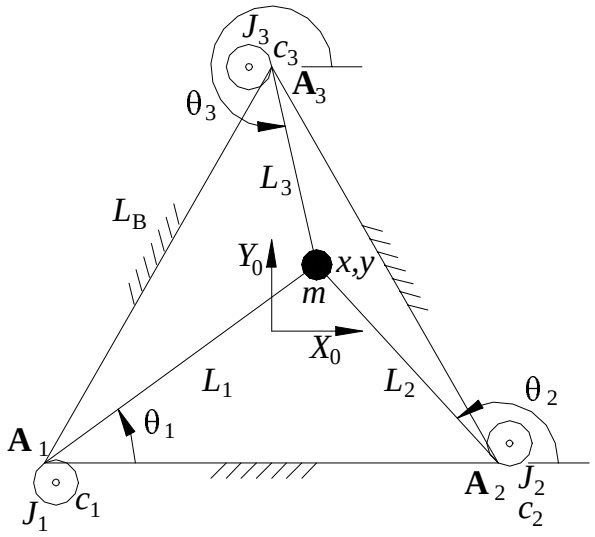

Figure 1. Planar 3-Cable CDDR Diagram

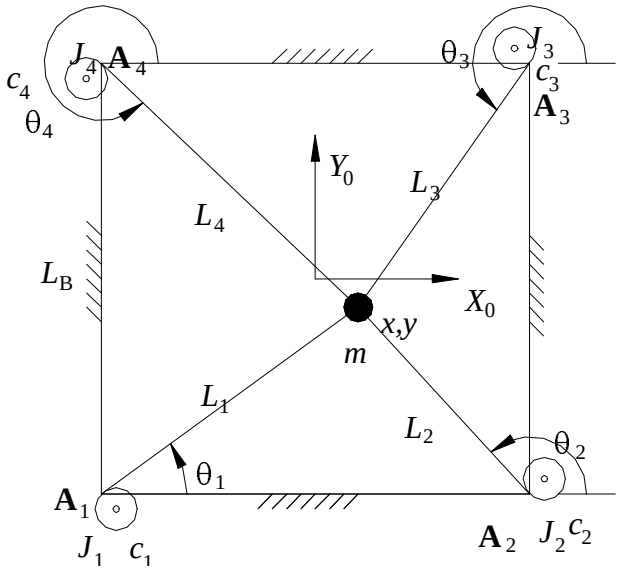

Figure 2. Planar 4-Cable CDDR Diagram

For the dynamics model derived in this section we assume that the CDDR cables are massless and perfectly stiff so we do not consider their inertias or spring stiffnesses. We further ignore the Coulomb friction and instead model linear viscous friction to account for the frictional losses. Despite these simplifications, the resulting model is coupled and nonlinear. We now present the Cartesian, actuator, and overall system dynamics models.

3.1 Cartesian Dynamics Model

The free-body diagram for the moving end-effector point is very simple and hence not shown. The 2-*dof* Cartesian dynamic model for the end-effector is given by:

$$\mathbf{m}\ddot{\mathbf{X}} = \mathbf{F} \tag{1}$$

where the Cartesian mass matrix is $\mathbf{m} = \begin{bmatrix} m & 0 \\ 0 & m \end{bmatrix}$, $\mathbf{X} = \{x \quad y\}^T$ is the end-effector position and $\mathbf{F}$ is the resultant of all n cable forces acting on the end-effector.

3.2 Actuator Dynamics Model

We also take into consideration the dynamic behavior of the lumped motor shaft/cable pulley; the free-body diagram for the i^{th} motor shaft/cable pulley subsystem is shown in Fig. 3. The combined motor shaft/cable pulley dynamics equations are expressed by the relationship:

$$\mathbf{J}\ddot{\boldsymbol{\beta}} + \mathbf{C}\dot{\boldsymbol{\beta}} = \boldsymbol{\tau} - r\mathbf{T} \tag{2}$$

where: $\mathbf{J} = \begin{bmatrix} J_1 & & 0 \\ & \ddots & \\ 0 & & J_n \end{bmatrix}$ and $\mathbf{C} = \begin{bmatrix} c_1 & & 0 \\ & \ddots & \\ 0 & & c_n \end{bmatrix}$

are diagonal matrices with rotational inertia and rotational viscous damping coefficients on the diagonal, all cable pulley radii are identical ($r_i = r$; $i = 1, \cdots, n$), $\boldsymbol{\tau} \in R^n$ is the vector of torques exerted by the motors, $\mathbf{T} \in R^n$ is the vector of cable tensions t_i, and $\boldsymbol{\beta} \in R^n$ is the vector of pulley angles. Since the cables can only exert positive tensions (they cannot push), to express the cable tensions as a function of the motor torques and angular motion from (2), we obtain:

$$\mathbf{T} = pos\left(\frac{1}{r}\left(\boldsymbol{\tau} - \mathbf{J}\ddot{\boldsymbol{\beta}} - \mathbf{C}\dot{\boldsymbol{\beta}}\right)\right) \tag{3}$$

where the symbol $pos()$ means we take the value of each vector component that is positive and we set to zero those components that were originally negative. Let us suppose that the torque on each motor is large enough to make all cables remain in tension at all times. Under this assumption:

$$\mathbf{T} = \frac{1}{r}\left(\boldsymbol{\tau} - \mathbf{J}\ddot{\boldsymbol{\beta}} - \mathbf{C}\dot{\boldsymbol{\beta}}\right) \tag{4}$$

3.3 System Dynamics Model

We now derive the overall system dynamics model by combining the Cartesian and actuator dynamics equations of motion. From the companion paper (Williams and Gallina, 2001), the statics relationship between forces on the end-effector and cable tensions is given by:

$$\mathbf{F} = \mathbf{S}\mathbf{T} \tag{5}$$

where the 2x*n* statics Jacobian matrix is:

$$\mathbf{S} = \begin{bmatrix} -\cos\theta_1 & \cdots & -\cos\theta_n \\ -\sin\theta_1 & \cdots & -\sin\theta_n \end{bmatrix} \tag{6}$$

where θ_i ($i = 1, \cdots, n$) are the cable angles (see Figs. 1 and 2).

We now need an inverse kinematics mapping relating the pulley angles β_i ($i = 1, \cdots, n$) expressed as functions of the end-effector position $\mathbf{X} = \{x \quad y\}^T$. Let us define all β_i to be zero when the end-effector is located at the origin of frame {**0**}. From this position, a right-handed positive angle β_i on one pulley will cause a negative change ΔL_i in cable length *i*: $\beta_i r = -\Delta L_i$. The change in cable length *i* is $\Delta L_i = L_i - L_{0i}$ where $L_i = \sqrt{(x - A_{ix})^2 + (y - A_{iy})^2}$ is the general length for cable *i* from the inverse position solution (Williams and Gallina, 2001) and $L_{0i} = \sqrt{(A_{ix})^2 + (A_{iy})^2}$ is the initial length for cable *i*. Therefore:

$$\boldsymbol{\beta} = \begin{Bmatrix} \beta_1(\mathbf{X}) \\ \vdots \\ \beta_n(\mathbf{X}) \end{Bmatrix} = \frac{1}{r} \begin{Bmatrix} L_{01} - \sqrt{(x - A_{1x})^2 + (y - A_{1y})^2} \\ \vdots \\ L_{0n} - \sqrt{(x - A_{nx})^2 + (y - A_{ny})^2} \end{Bmatrix} \tag{7}$$

Successive time derivatives of (7) yield:

$$\begin{aligned} \dot{\boldsymbol{\beta}} &= \frac{\partial \boldsymbol{\beta}}{\partial \mathbf{X}} \dot{\mathbf{X}} \\ \ddot{\boldsymbol{\beta}} &= \frac{d}{dt}\left(\frac{\partial \boldsymbol{\beta}}{\partial \mathbf{X}}\right)\dot{\mathbf{X}} + \frac{\partial \boldsymbol{\beta}}{\partial \mathbf{X}} \ddot{\mathbf{X}} \end{aligned} \tag{8}$$

where:

$$\frac{\partial \boldsymbol{\beta}}{\partial \mathbf{X}} = -\frac{1}{r} \begin{bmatrix} \dfrac{x - A_{1x}}{L_1} & \dfrac{y - A_{1y}}{L_1} \\ \vdots & \vdots \\ \dfrac{x - A_{nx}}{L_n} & \dfrac{y - A_{ny}}{L_n} \end{bmatrix} \tag{9}$$

and $L_i = \sqrt{(x - A_{ix})^2 + (y - A_{iy})^2}$ is the length of cable *i*, a function of $\mathbf{X} = \{x \quad y\}^T$. By substituting (8) into (4) we obtain:

$$\mathbf{T} = \frac{1}{r}\left(\boldsymbol{\tau} - \mathbf{J}\left(\frac{d}{dt}\frac{\partial \boldsymbol{\beta}}{\partial \mathbf{X}}\dot{\mathbf{X}} + \frac{\partial \boldsymbol{\beta}}{\partial \mathbf{X}}\ddot{\mathbf{X}}\right) - \mathbf{C}\frac{\partial \boldsymbol{\beta}}{\partial \mathbf{X}}\dot{\mathbf{X}}\right) \tag{10}$$

Finally, by combining (1), (5), and (10), we obtain the overall dynamics equations of motion, expressed in a standard Cartesian form for robotic systems (Lewis et al., 1993):

$$\mathbf{M}_{eq}(\mathbf{X})\ddot{\mathbf{X}} + \mathbf{N}(\mathbf{X}, \dot{\mathbf{X}}) = \mathbf{S}(\mathbf{X})\boldsymbol{\tau} \tag{11}$$

where:

$$\mathbf{M}_{eq} = r\mathbf{m} + \mathbf{S}(\mathbf{X})\mathbf{J}\frac{\partial \boldsymbol{\beta}}{\partial \mathbf{X}} \tag{11a}$$

$$\mathbf{N}(\mathbf{X}, \dot{\mathbf{X}}) = \mathbf{S}(\mathbf{X})\left(\mathbf{J}\frac{d}{dt}\frac{\partial \boldsymbol{\beta}}{\partial \mathbf{X}} + \mathbf{C}\frac{\partial \boldsymbol{\beta}}{\partial \mathbf{X}}\right)\dot{\mathbf{X}} \tag{11b}$$

Note the statics Jacobian matrix $\mathbf{S} = \mathbf{S}(\mathbf{X})$ from (6) is a function of Cartesian position $\mathbf{X} = \{x \quad y\}^T$ through the cable angles $\theta_i = \tan^{-1}\left(\dfrac{y - A_{iy}}{x - A_{ix}}\right)$ (see Figs. 1 and 2).

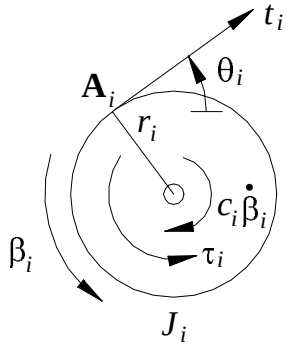

Figure 3. Free-Body Diagram for the i^{th} Pulley/Shaft

4. CDDR CONTROLS SIMULATION

This section presents our control architecture for planar CDDRs based on the overall system Cartesian dynamics equations of motion (11). The input to the plant is the vector of torques $\boldsymbol{\tau}$. Each component of $\boldsymbol{\tau}$ has to be positive or zero at the minimum (in practice, a small positive value). In order to avoid this problem, let us introduce a virtual Cartesian force input $\mathbf{F}_V$:

$$\mathbf{F}_V = \mathbf{S}(\mathbf{X})\boldsymbol{\tau} \tag{12}$$

Since the statics Jacobian matrix **S**(**X**) has dimension 2x*n*, this virtual force input $\mathbf{F}_V$ has the dimension of the Cartesian space, 2 in this paper. The components of $\mathbf{F}_V$ are not restricted to be positive. If we can develop a control law for the virtual Cartesian force input $\mathbf{F}_V$, it is always possible to find a real controls torque input $\boldsymbol{\tau}$ with all positive components that satisfies (12), if the CDDR position is within the statics workspace. In Williams and Gallina (2001) we prove that the entire base polygon is within the statics workspace for planar CDDRs with regular convex base polygons. Therefore, for control law development, we can consider the new dynamic equation:

$$\mathbf{M}_{eq}(\mathbf{X})\ddot{\mathbf{X}} + \mathbf{N}(\mathbf{X}, \dot{\mathbf{X}}) = \mathbf{F}_V \tag{13}$$

In this paper we ignore the nonlinear dynamics terms $\mathbf{N}(\mathbf{X}, \dot{\mathbf{X}})$, we use the commanded (reference) Cartesian acceleration $\ddot{\mathbf{X}}_R$ in a feedforward term, and we implement a Cartesian PD controller to reduce the tracking error $\mathbf{e} = \mathbf{X}_R - \mathbf{X}$. The commanded (reference) Cartesian position is $\mathbf{X}_R = \{x_R \quad y_R\}^T$. The control law for the virtual Cartesian force input $\mathbf{F}_V$ is:

$$\mathbf{F}_V = \mathbf{M}_{eq}(\mathbf{X}_R)\ddot{\mathbf{X}}_R + \mathbf{K}_P\mathbf{e} + \mathbf{K}_D\dot{\mathbf{e}} \qquad (14)$$

The control architecture (shown in the block diagram of Fig. 4) is made up of three different parts: the PD controller, the feedforward term, and the virtual-Cartesian-force-input-to-real-actuator-torque calculation. In this paper the PD controller gains are determined via trial-and-error using a *Matlab Simulink* simulation to achieve reasonable performance. The matrix gains $\mathbf{K}_P$,$\mathbf{K}_D$ are 2x2 diagonal matrices, which means that the PD control is accomplished independently for the *x* and *y* motions, even though the dynamics model is coupled. The feedforward term $\mathbf{M}_{eq}(\mathbf{X}_R)\ddot{\mathbf{X}}_R$ is composed of the overall position-dependent Cartesian mass matrix and the reference Cartesian acceleration components. The virtual-to-real calculation has the problem to invert the matrix **S**(**X**) that is non-square and such that only positive cable tensions result. This problem is solved in the companion paper (Williams and Gallina, 2001).

We do not generally have access directly to Cartesian position **X** feedback via a sensor. Instead, we must calculate this feedback using the encoder feedback for each cable pulley angle β_i to determine the cable lengths L_i; these lengths are then used as the inputs to the forward position kinematics solution (Williams and Gallina, 2001) to calculate Cartesian position **X** for feedback in the control architecture. This feedback scheme will work well only if sufficient tension is maintained on all cables at all times.

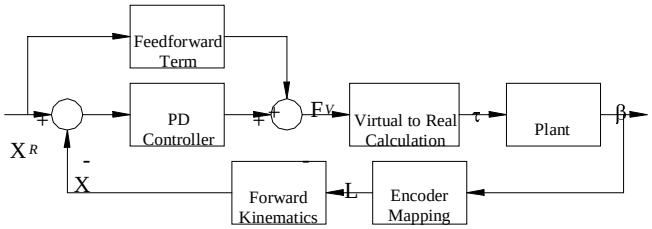

Figure 4. Control Architecture for Planar CDDRs

5. EXAMPLES

This section presents controls simulation examples using the dynamics equations of motion for the planar 3-cable CDDR with one degree of actuation redundancy and for the planar 4-cable CDDR with two degrees of actuation redundancy. The circle-tracing task is identical to that presented in the examples of the companion paper (Williams and Gallina, 2001), but now dynamics and control is considered. The base equilateral triangle side is L_B = 1 *m* and the base square side is L_B = 0.6580 *m*.

The simulated task is for the CDDR end-effector point $\mathbf{X} = \{x \quad y\}^T$ to trace a circle in the plane. Unlike the kinematics and statics example task in the companion paper, the constant Cartesian force $\mathbf{F}_R$ on the environment will be set to zero. The identical task will be performed by both 3-cable and 4-cable CDDRs, both without and with the feedforward term, and the results will be compared. The circle is centered at the base polygon centroid (the origin of {**0**}) and the circle radius is arbitrarily chosen to be three-quarters of the shortest distance from the base triangle centroid to a triangle side: *r* = 0.2165 *m*. Figures 5 and 6 show the simulated task to scale for the 3- and 4-cable cases, respectively, at the starting (and ending) point.

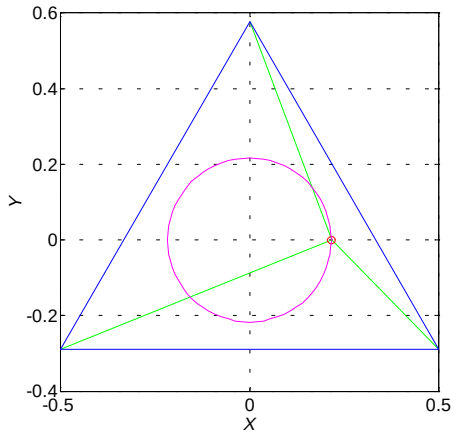

Figure 5. Planar 3-Cable CDDR Example Task

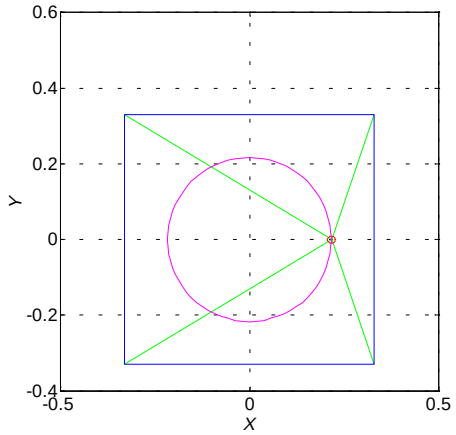

Figure 6. Planar 4-Cable CDDR Example Task

We define polar angle ϕ as the independent parameter for the circle; it is measured using the right-hand from the right horizontal to the current circle radius; ϕ is shown as 0 (and 360°) in Figs. 5 and 6. In the simulated task, one circle revolution is traced out in 1 *sec*. We provide a constant acceleration for the first half of the circle and an equal constant deceleration for the second half of the circle; the motion starts and ends at zero velocity. The kinematic task relationships for this desired reference motion are $\alpha = \dot{\omega} = \ddot{\phi} = 8\pi$, $\omega = \dot{\phi} = \alpha t$, and $\phi = \alpha t^2/2$ for the first half of the circle; the second half is symmetric to the first. Figures 7a and 7b show the associated commanded (reference) Cartesian position $\mathbf{X}_R$ and Cartesian acceleration $\ddot{\mathbf{X}}_R$ for use in the feedforward term.

The parameters for the dynamics equations of motion (11) for both the 3- and 4-cable CDDRs are: point mass *m* = 1 *kg*; rotational shaft/pulley inertias $J_i = 0.0008$ kgm^2 (for all $i = 1,\cdots,n$); shaft rotational viscous damping coefficients $c_i = 0.01$ *Nms* (for all $i = 1,\cdots,n$); and $r_i = r = 5$ *cm* (for all $i = 1,\cdots,n$). The same Cartesian PD controller is used for both CDDRs, found by trial-and-error using the *Simulink* simulation: gain $\mathbf{K}_P$ is a 2x2 diagonal matrix with equal gains of $K_P = 2000$ on the diagonal, and gain $\mathbf{K}_D$ is a 2x2 diagonal matrix with equal gains of $K_D = 10$ on the diagonal.

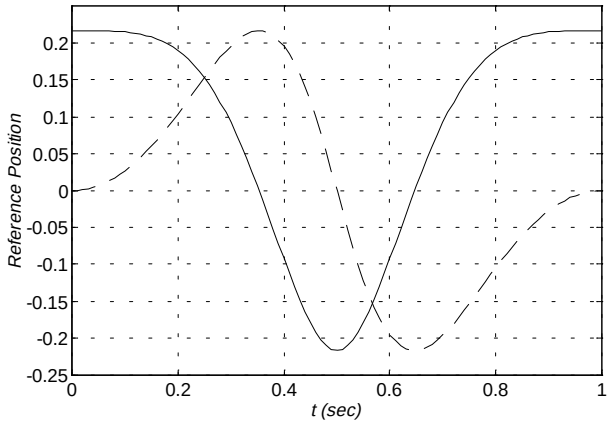

Figure 7a. Reference Position x_R (solid) *and* y_R (dash) (*m*)

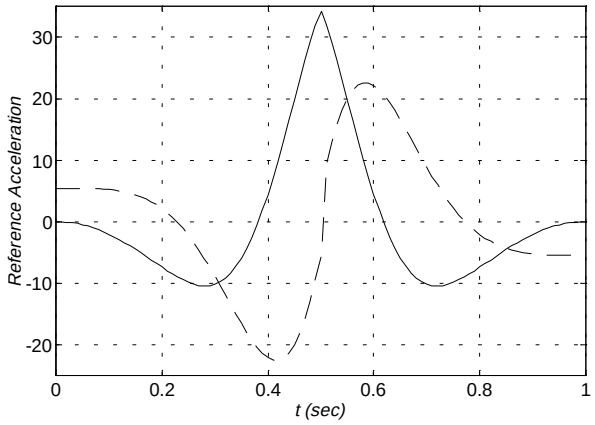

Figure 7b. Reference Acceleration $\ddot{x}_R$ (solid) *and* $\ddot{y}_R$ (dash) (m/s^2)

Four control simulations of the dynamics model are presented in this section: the 3-cable and 4-cable CDDRs, both without and with the feedforward term in the block diagram of Fig. 4. Figure 8 shows the circle trajectory tracking error $\mathbf{e} = \mathbf{X}_R - \mathbf{X}$ for the 3-cable CDDR without the feedforward controller term. Figure 9a shows the tracking error for the 3-cable CDDR with the feedforward controller term included.

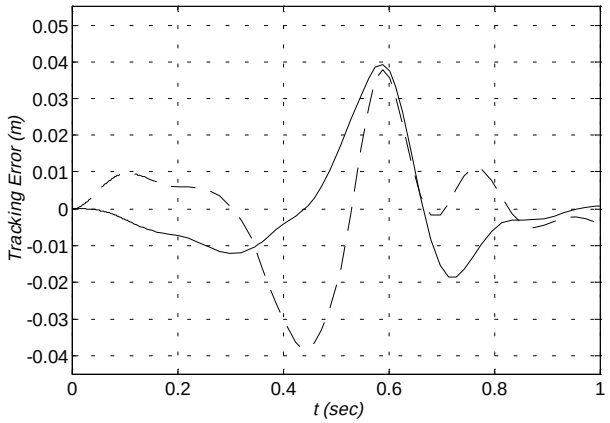

Figure 8. 3-cable CDDR Tracking Error, without Feedforward e_x (solid) *and* e_y (dash)

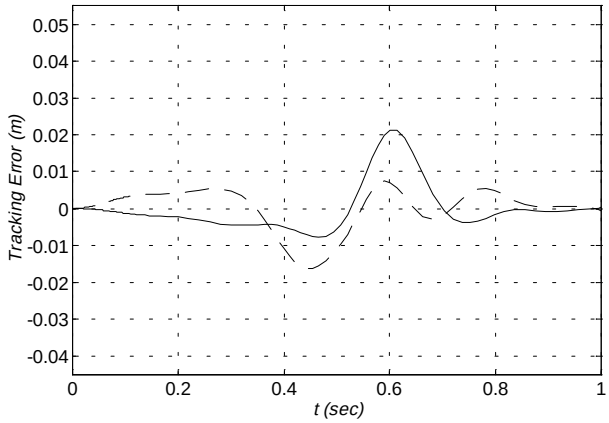

Figure 9a. 3-cable CDDR Tracking Error, with Feedforward e_x (solid) *and* e_y (dash)

The feedforward term has cut the tracking error nearly in half: without feedforward the peak errors were approximately ±4 *cm*, and with feedforward the peak errors were approximately ±2 *cm*. For both cases, the peak errors occurred after the halfway point in the circle, when the velocity is the greatest. This is expected since we ignore the nonlinear dynamics terms $\mathbf{N}(\mathbf{X},\dot{\mathbf{X}})$ for both cases. The tracking error is small for the non-feedforward case at the end of the circle motion (when the velocity is supposed to go back to zero); the tracking error is better, nearly zero, for the feedforward case at the end of the circle motion.

Since the tracking error with the feedforward term included is clearly preferable, we now show more control details for this case. Figure 9b shows the virtual Cartesian force input $\mathbf{F}_V$, Fig. 9c shows the three cable tensions, and Fig. 9d shows the three actuator torques for the prescribed dynamic circular motion.

For the control we have specified a minimum cable tension of 1 *N*, rather than zero, in attempt to avoid conditions where one or more cables go slack. Despite this, all three cable tensions dip below zero in Fig. 9c at different times, due to dynamics. We are currently developing a method to avoid this problem by estimating the required minimum tensions on-line to avoid slack cables considering dynamics. Note that all simulated actuator torques remain positive, despite the small cable tension problem.

The virtual Cartesian force inputs, cable tensions, and actuator torques of Figs. 9b-9d show these variables for the feedforward case. The equivalent plots for the non-feedforward case are not shown to save space. However, the dependent axis ranges in Figs. 9b-9d were chosen such that the non-feedforward cases (not shown) just fit. From this we can conclude that the virtual Cartesian force inputs, cable tensions, and actuator torques for the control with feedforward are significantly less than for the same variables in the non-feedforward case. Therefore, due to better tracking error and reduced forces, tensions, and torques, the control architecture including the feedforward term is superior, despite the additional preparation and controller cost. These two paragraphs of results discussion for the 3-cable CDDR also extend to the four cable CDDR, as will be seen next.

The tracking error in these examples is rather large (several *cm*). Our intent is to validate the theoretical work via experimental results, and then develop improved control to reduce this tracking error. Thus, we need a sizable tracking error that we can measure in the lab.

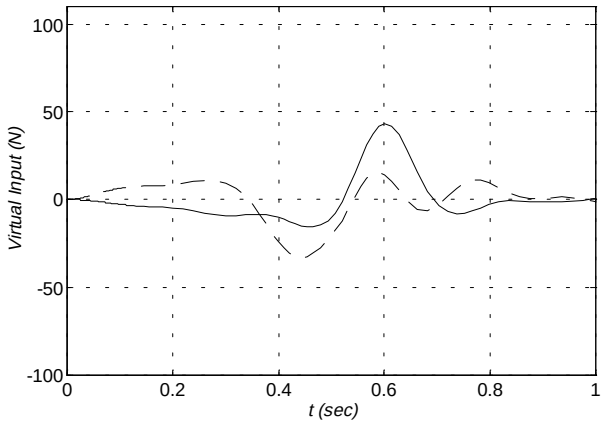

Figure 9b. 3-cable CDDR Virtual Input, with Feedforward F_{Vx} (solid) *and* F_{Vy} (dash)

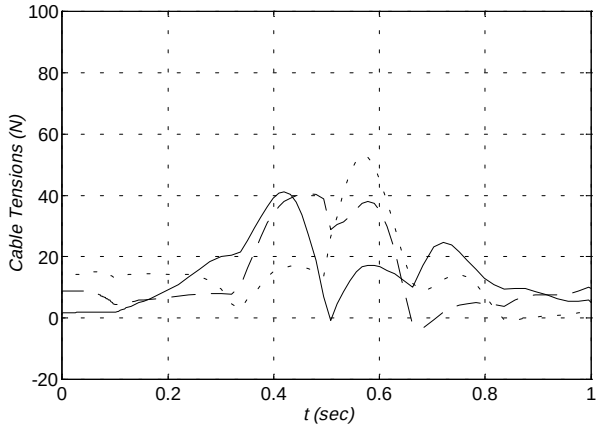

Figure 9c. 3-cable CDDR Cable Tensions, with Feedforward t_1 (solid), t_2 (long dash), and t_3 (short dash)

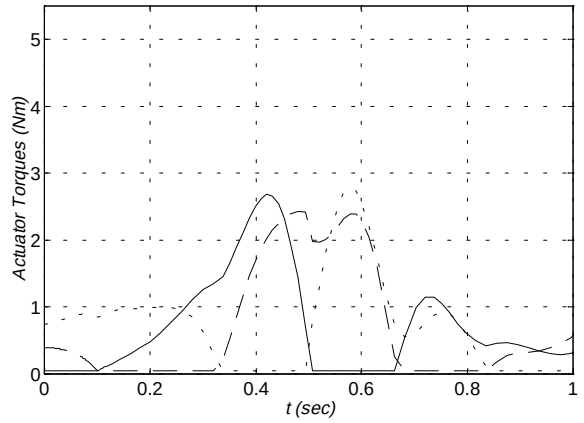

Figure 9d. 3-cable CDDR Actuator Torques, with Feedforward τ_1 (solid), τ_2 (long dash), and τ_3 (short dash)

For comparison purposes, the same types of results are now shown, for simulated control of the 4-cable CDDR. Figure 10 shows the tracking error $\mathbf{e} = \mathbf{X}_R - \mathbf{X}$ for the 4-cable CDDR without the feedforward controller term. Figure 11a shows the tracking error for the 4-cable CDDR with the feedforward controller term included.

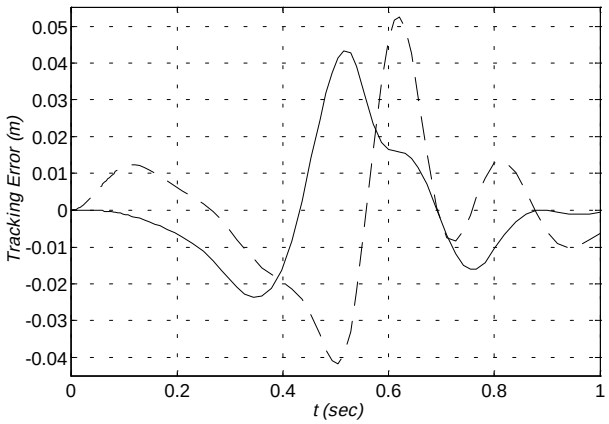

Figure 10. 4-cable CDDR Tracking Error, without Feedforward e_x (solid) *and* e_y (dash)

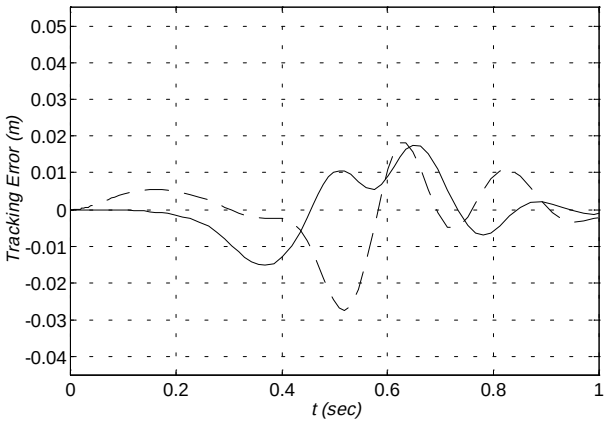

Figure 11a. 4-cable CDDR Tracking Error, with Feedforward e_x (solid) *and* e_y (dash)

Again, the tracking error was cut nearly in half by using the feedforward term, so we now show more control details for this case. Figure 11b shows the virtual Cartesian force input $\mathbf{F}_V$, Fig. 11c shows the four cable tensions, and Fig. 11d shows the four actuator torques for the prescribed dynamic circular motion.

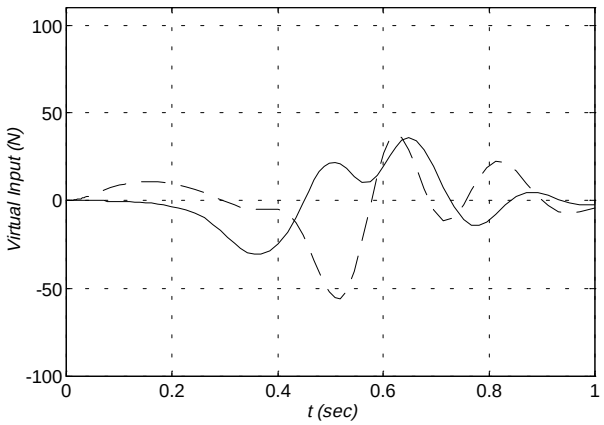

Figure 11b. 4-cable CDDR Virtual Input, with Feedforward F_{Vx} (solid) *and* F_{Vy} (dash)

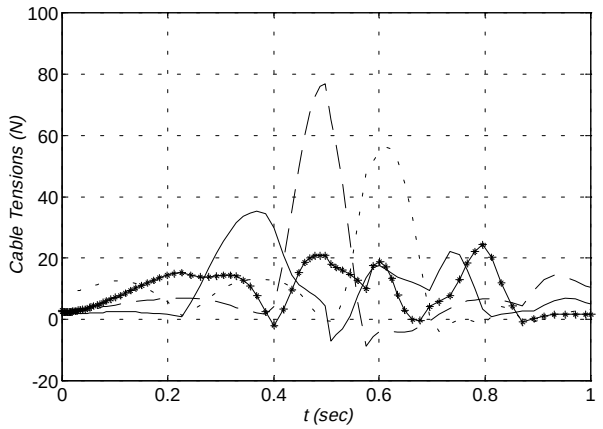

Figure 11c. 4-cable CDDR Cable Tensions, with Feedforward t_1 (solid), t_2 (long dash), t_3 (short dash), and t_4 (asterisk)

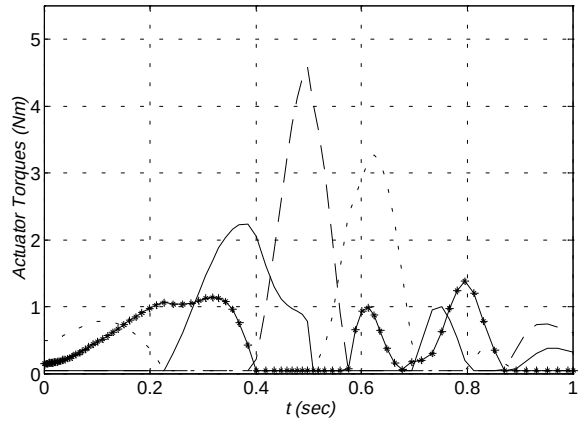

Figure 11d. 4-cable CDDR Actuator Torques, with Feedforward τ_1 (solid), τ_2 (long dash), τ_3 (short dash), and τ_4 (asterisk)

The tracking errors for the 4-cable CDDR (without and with the feedforward term) are worse than those of the 3-cable CDDR. This is due to the fact that, though we scaled the kinematics workspace so that both 3- and 4-cable CDDRs had the same area, we did not scale the actuator inertias, and the 4-cable CDDR has a fourth equal-sized shaft inertia which makes the tracking error larger. Also, the 4-cable CDDR cable tensions and actuator torques are higher than those for the 3-cable CDDR with the same type of control (with the feedforward term). The virtual Cartesian force input for both CDDRs are similar since it is a Cartesian controller.

Remember that no external force was specified to exert on the environment during the dynamic circular motion. From the companion paper (Williams and Gallina, 2001), it was found that for pseudostatic motion conditions, the required 4-cable CDDR cable tensions were significantly lower than those required by the 3-cable CDDR for exerting forces on the environment, so the 4-cable dynamics results will not be as bad when considering a static load to exert.

Like the 3-cable CDDR results shown in Figs. 9 above, Figs. 11 also display the following: due to dynamics, some cable tensions dip below zero, even though we specify a minimum cable tension of 1 *N* on all cables at all times. Again, this does not occur for the simulated actuator torques. Also, the magnitude of the virtual Cartesian force inputs, cable tensions, and actuator torques of Figs. 11b-11d, representing the feedforward case, are less than those without the feedforward term (not shown). However, the peak values for cable tensions and actuator torques approach more nearly the cases without the feedforward term (as seen by the scale on the independent axes, which were set for the non-feedforward cases) than the 3-cable CDDR did. It is still clear that the controller including the feedforward term is superior to the controller without the feedforward term.

6. CONCLUSION

This paper performs dynamics modeling and control simulation for a proposed hybrid parallel/serial manipulator architecture wherein the translational freedoms are provided by a parallel cable-direct-driven robot (CDDR) and the rotational freedoms are provided by a serial wrist mechanism. The motivation behind this work is to improve the serious cable interference and negative cable tensions possible with existing CDDRs that guide both translational and rotational freedoms. Dynamics modeling is required to achieve high velocities and accelerations in translational motion. A controls simulation example is presented comparing the dynamics of planar 3- and 4-cable CDDRs performing the same task.

Only the translational motion is considered in this paper. It was found that the tracking error of the 4-cable CDDR was higher than that of the 3-cable CDDR, due to the added inertia of an extra actuator shaft/cable pulley. In both CDDRs, the cable tensions became negative (slack) due to dynamics in small ranges of the motion despite the prescribed controller minimum of 1 *N* tension on each cable. From comparing simulated performance, the controller with the feedforward term proved to be superior to the controller without the feedforward term for both 3- and 4-cable CDDRs.

Our future work plans include more complete dynamics modeling (cable inertia and stiffness, Coulomb friction, among others), development of a method to avoid slack cables based on dynamics, improved nonlinear controller development, hardware implementation, and experimental validation of our results.

REFERENCES

P.D. Campbell, P.L. Swaim, and C.J. Thompson, 1995, "*Charlotte Robot Technology for Space and Terrestrial Applications*", 25th International Conference on Environmental Systems, San Diego, SAE Article 951520.

C.M. Gosselin, 1996, "Parallel Computation Algorithms for the Kinematics and Dynamics of Planar and Spatial Parallel Manipulators", *Journal of Dynamic Systems, Measurement, and Control*, 118(1): 22-28.

F.L. Lewis, C.T. Abdallah, and D.M. Dawson, 1993, Control of Robot Manipulators, MacMillan, New York.

R.G. Roberts, T. Graham, and T. Lippitt, 1998, "*On the Inverse Kinematics, Statics, and Fault Tolerance of Cable-Suspended Robots*", Journal of Robotic Systems, 15(10): 581-597.

M. Sklar and D. Tesar, 1988, *"Dynamic Analysis of Hybrid Serial Manipulator Systems Containing Parallel Modules"*, Journal of Mechanisms, Transmissions, and Automation in Design, 110(2): 109-115.

L.W. Tsai, 1999, Robot Analysis: The Mechanics of Serial and Parallel Manipulators, Wiley, New York.

R.L. Williams II and P. Gallina, 2001, *"Planar Cable-Direct-Driven Robots, Part I: Kinematics and Statics"*, submitted to the 2001 ASME Design Technical Conferences, September 9-12, Pittsburgh, PA.